EPJ Web of Conferences **29**, 00040 (2012)
DOI: 10.1051/epjconf/20122900040

The Structural and magnetic properties of $Bi_{1-x}A_xFe_{1-y}B_yO_3$ multiferroic system

A. Al-Sharif [a] and A. Al-Muqri

Dept. of physics, Mu'tah University – Al-Karak- JORDAN

Abstract. We have prepared $Bi_{1-x}A_xFe_{1-y}B_yO_3$, where A=Ca or Gd and B=Ni or Zn. The solid state reaction technique was used to prepare the samples. The effects of the mentioned elemental substitution on the structural and magnetic properties of the multiferroic compound prepared are reported.
Keywords: BiFO multiferroic, hysteresis loop, x-ray diffraction.

1. Introduction

Bismuth ferrite ($BiFeO_3$) referred to as BFO has perovskite structure. It is a G-type canted antiferromagnetic with a transition temperature (T_N = 643K), and a ferroelectric with a transition temperature (T_C = 1103 K), which make it a candidate multiferroic material for various applications. It is one of the most promising lead-free piezoelectric materials by exhibiting multiferroic properties at room temperature. However BFO has some inherent problems such as preparation of the phase pure compound, a high leakage current and wide difference in ferroic transition temperatures. Recently different synthesis processes have been adopted to get single phase formation of BFO [1-5]. However, in pure BFO ceramics high value macroscopic magnetization could not be achieved. Several attempts have been made to solve these problems by suitable modifications at the Bi and/or Fe sites or fabrication of composites.

Attempts to improve the BFO properties have been made by doping it with rare earth elements such as lanthanum (La), samarium (Sm), gadolinium (Gd), terbium (Tb) and dysprosium (Dy) etc [6-15]. The dopant can be at the A-site or the B-site. A-site being the edges of the perovskite cell and the B-site being the centre of the perovskite cell. The aim of this research is to prepare using the conventional ceramic technique $Bi_{1-x}A_xFe_{1-y}B_yO_3$ ceramics where (A= Ca or Gd) and (B= Ni or Zn) are the substitution elements in the Bi-site and Fe-site respectively, while (x=0.1 and y=0, 0.02) are the concentration values of the doping elements. The effect of the proposed substitution on the structural and magnetic properties of our ceramics will be reported and explained.

2 Experimental Technique

The samples were prepared using the solid-state reaction method. Bi_2O_3, Fe_2O_3, Gd_2O_3, CaO, ZnO or NiO powders with 99% purity or better were used. According to the required stoichiometry, the powders were weighed, mixed, and ground in order to get a homogeneous mixture. The mixtures

[a] e-mail : latif45@hotmail.com

were then calcinated at 825°C in a Carbolite tube furnace for 4h. After calcination, each sample was slowly cooled to room temperature while it was inside the furnace. The process was repeated once more.

The X-ray diffraction (XRD) patterns were recorded using a Seifert 3003 TT diffractometer with CuK_α radiation (λ = 1.5406 Å). The Miller indices (*hkl*) of the diffraction peaks were referred to hexagonal axes rather than rhombohedral axes [11].

The magnetic measurements were performed on samples of equal mass using a 9600 LDJ Vibrating Sample Magnetometer (VSM), which was calibrated using a Ni standard.

3. Experimental Results

3.1. Structural measurements

X-ray diffraction pattern of Ca-doped $BiFeO_3$ samples are shown in figure 1. All the samples give X-ray peaks corresponding to the rhombohedral perovskite-like $BiFeO_3$ phase. Besides the formation of this phase, all samples show small amounts of the non-perovskite $Bi_2Fe_4O_9$ phase (marked by *) and the cubic $Bi_{25}FeO_{40}$ phase (marked by #). The existence of $Bi_2Fe_4O_9$ and $Bi_{25}FeO_{40}$ as impurity phases in doped bismuth ferrite samples have been reported by several authors [15-17]. The main peaks of the $Bi_{0.9}Ca_{0.1}FeO_3$ sample, indexed on the figure, match well with the standard $BiFeO_3$ peak positions with CuK_α radiation. The lattice parameters *a* and *c* (equivalent to hexagonal), the volume of the unit cell *V*, and the ratio *c/a (lattice distortion)* for the compounds studied are listed in table (1).

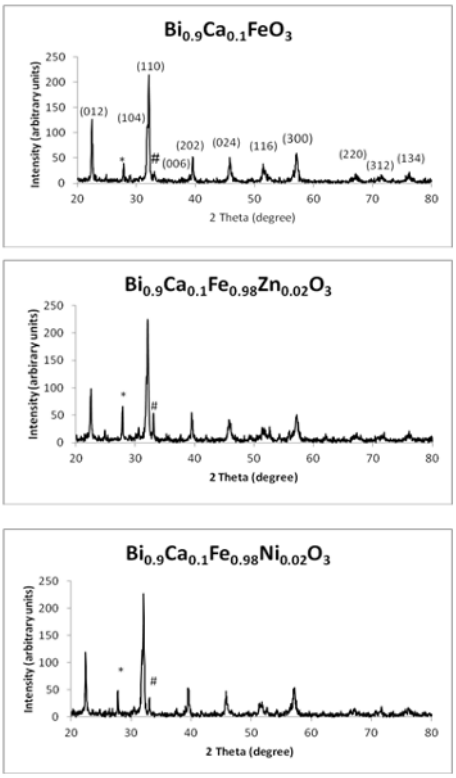

Figure 1: The XRD of the Ca-doped sampes

Table 1. Some structural parameters of the Ca-doped $BiFeO_3$ compounds

Compound	*a* (Å)	*c* (Å)	*V* (Å^3)	*c/a*
$Bi_{0.9}Ca_{0.1}FeO_3$	5.5710	13.7875	370.6	2.4749
$Bi_{0.9}Ca_{0.1}Fe_{0.98}Zn_{0.02}O_3$	5.5767	13.7887	371.3	2.4726
$Bi_{0.9}Ca_{0.1}Fe_{0.98}Ni_{0.02}O_3$	5.5722	13.8131	371.4	2.4789

X-ray diffraction patterns of the Gd-doped $BiFeO_3$ samples (figure 2) indicate the presence of bismuth ferrite impurity phase $Bi_2Fe_4O_9$ (marked by *), a small amount of $Bi_{25}FeO_{40}$ phase (marked by #) and other impurity phase(s) (marked by ^) along with the major $BiFeO_3$ phase. All the samples were indexed according to the crystal structure of pure BiFeO3. The impurity phases $Bi_2Fe_4O_9$ and $Bi_{25}FeO_{40}$ were identified by their standard peak positions with CuK_α radiation. It was not possible, however, to achieve phase purity for our samples even by longer calcination times (which could also lead to more volatilization of Bi_2O_3). The presence of impurity phases in the Gd^{3+} doped samples is most probably due to the large atomic weight of gadolinium, which does not allow it to interact easily and quickly, leading to impurity formation. The structural parameters for the studied compounds are listed in table 2.

Table 2. Some structural parameters of the Gd-doped $BiFeO_3$ compounds

Compound	*a* (Å)	*c* (Å)	*V* (Å^3)	*c/a*
$Bi_{0.9}Gd_{0.1}FeO_3$	5.5729	13.8799	373.3	2.4906
$Bi_{0.9}Gd_{0.1}Fe_{0.98}Zn_{0.02}O_3$	5.5606	13.8439	370.7	2.4896
$Bi_{0.9}Gd_{0.1}Fe_{0.98}Ni_{0.02}O_3$	5.5731	13.8931	373.7	2.4929

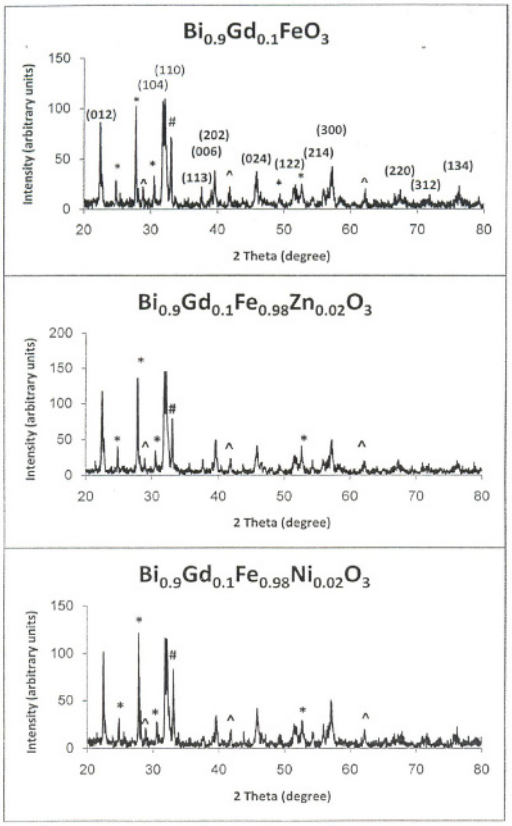

Fig. 2. The XRD of the Gd-doped samples

3.2. Magnetic properties

The room temperature magnetic hysteresis loops of the Ca doped compounds are shown in figure 3.

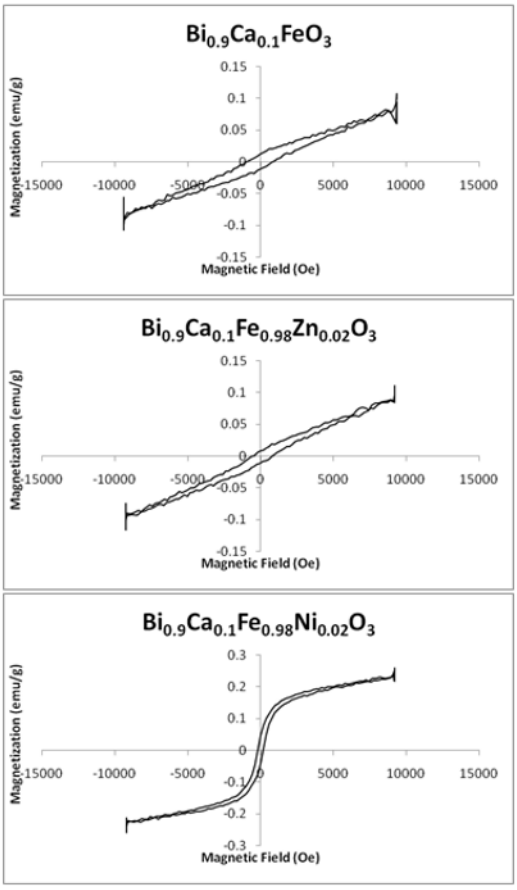

Fig. 3. The hysteresis loops of the Ca-doped compounds

All the samples illustrate weak ferromagnetism with no saturation magnetization. The main sample ($Bi_{0.9}Ca_{0.1}FeO_3$) has the greatest coercivity field value H_c, (table 3).

Table 3. Some magnetic parameters of the Ca-doped $BiFeO_3$ ceramics

Compound	H_c (kOe)	M_s (emu/g)	M_r (emu/g)
$Bi_{0.9}Ca_{0.1}FeO_3$	0.865	9.88 x10^{-2}	1.18 **x** 10^{-2}
$Bi_{0.9}Ca_{0.1}Fe_{0.98}Zn_{0.02}O_3$	0.690	9.90 x 10^{-2}	9.62 x 10^{-3}
$Bi_{0.9}Ca_{0.1}Fe_{0.98}Ni_{0.02}O_3$	0.183	2.52 x 10^{-1}	4.20 **x** 10^{-2}

Doping the B-site with nickel enhances the magnetization and gives a narrower loop with small coercivity value when compared to the basis sample. We couldn't achieve magnetically saturated loops for any of the studied samples so the saturation magnetization values obtained and listed in the magnetic properties tables below represent the magnetization at the highest field used (1Tesla). The saturation magnetization is dependent only on the magnitude of the atomic magnetic moments *m* and the number of atoms per unit volume *n* [18]. Although Zn^{2+} and Ni^{2+} are both transition metal ions , Zn^{2+} ion is a diamagnetic ion, while Ni^{2+} is a magnetically active ion and has a magnetic moment ($\mu_{eff} = 3.2\mu_B$). In $BiFeO_3$ the spin is provided by the transition metal ion Fe^{3+}, doping with a foreign

transition metal such as Ni^{2+} increases the effective magnetic moment in the B-site and hence increases the maximum magnetization of the basis compound. This rise in maximum magnetization is associated with a decrease in coercivity which is due to the decrease in the magnetocrystalline anisotropy.

The substitution with divalent cations in Fe site decreases the anisotropy. In bismuth ferrite the Fe magnetic moments are coupled ferromagnetically within the pseudocubic [111] planes and antiferromagnetically between adjacent planes (so-called G-type antiferromagnetic order). If the magnetic moments are oriented perpendicular to the [111] direction, the symmetry permits a canting of the antiferromagnetic sublattices resulting in a macroscopic magnetization, (so-called weak ferromagnetism). However, superimposed on the antiferromagnetic ordering, there is a spiral spin structure in which the antiferromagnetic axis rotates through the crystal with an incommensurate long-wavelength period of 620Å. This spiral spin structure leads to a cancellation of the macroscopic magnetization and also inhibits the observation of the linear magnetoelectric effect [11]. The cancellation of magnetization caused by the spiral spin structure ordering can be improved by doping foreign transition metal ions. In this system, spontaneous magnetization observed in Fe-substituted compounds either by Zn^{2+} or Ni^{2+} is due to the substitution-induced suppression of the spiral spin modulation. Further, the charge compensation due to substitution of Bi^{3+} by Ca^{2+} (an ion with different oxidation number) can be achieved by the formation of oxygen vacancies. This charge imbalance has to be compensated by oxygen deficiency ($O_{3-\delta}$ instead of O_3), however it is difficult to draw a clear conclusion without magnetic neutron diffraction or other structural studies on these divalent doped compounds.

For the Gd doped system, all samples show unsaturated hysteresis loops with small remnant magnetization as shown in figure 4. $Bi_{0.9}Gd_{0.1}FeO_3$ compound has the greatest coercive field value in this group, (table 4).

Table 4. Some magnetic parameters of the Gd-doped $BiFeO_3$ ceramics

Compound	H_c (kOe)	M_s (emu/g)	M_r (emu/g)
$Bi_{0.9}Gd_{0.1}FeO_3$	0.807	2.36×10^{-1}	2.36×10^{-2}
$Bi_{0.9}Gd_{0.1}Fe_{0.98}Zn_{0.02}O_3$	0.619	2.12×10^{-1}	2.04×10^{-2}
$Bi_{0.9}Gd_{0.1}Fe_{0.98}Ni_{0.02}O_3$	0.301	1.87×10^{-1}	3.30×10^{-2}

Doping with nickel increases the remnant magnetization and decreases the coercivity field value; this behavior is similar to that of the Ca-doped samples. Previous studies [19,20] showed that the most effective way to induce spontaneous magnetization in $BiFeO_3$ should be related to the substitution with ions possessing a large difference in ionic radius with respect to that of Bi^{3+} (r_{Bi} =1.17Å) such as Gd^{3+}(r_{Gd} =1.053Å). In $Bi_{0.9}Gd_{0.1}FeO_3$ the reduction in the average ionic radius of Bi site with 1% leads to a larger distortion of $BiFeO_3$. The lattice distortion results in stronger canting of spins; this explains why the antiferromagnetic $BiFeO_3$ shows large net magnetization with doping Gd^{3+} ions in the Bi site. Furthermore, the co-doping of the magnetically active Gd^{3+} in the A-site of bismuth ferrite with the ferromagnetic Ni^{2+} in the B-site drastically changes the magnetic properties of $BiFeO_3$ and leads to stronger A-B magnetic interactions, since Bi-site average ionic radius $<r_A>$ is decreased, the effective magnetic moment of the Bi-site ion is increased (the effective number of Bohr magneton for Gd^{3+} is 8.0), and the effective magnetic moment of the Fe-site ion is increased (the effective number of Bohr magneton for Ni^{2+} is 3.2). The widening of the hysteresis loops observed in the Gd-doped samples is also due to the presence of impurity phases.

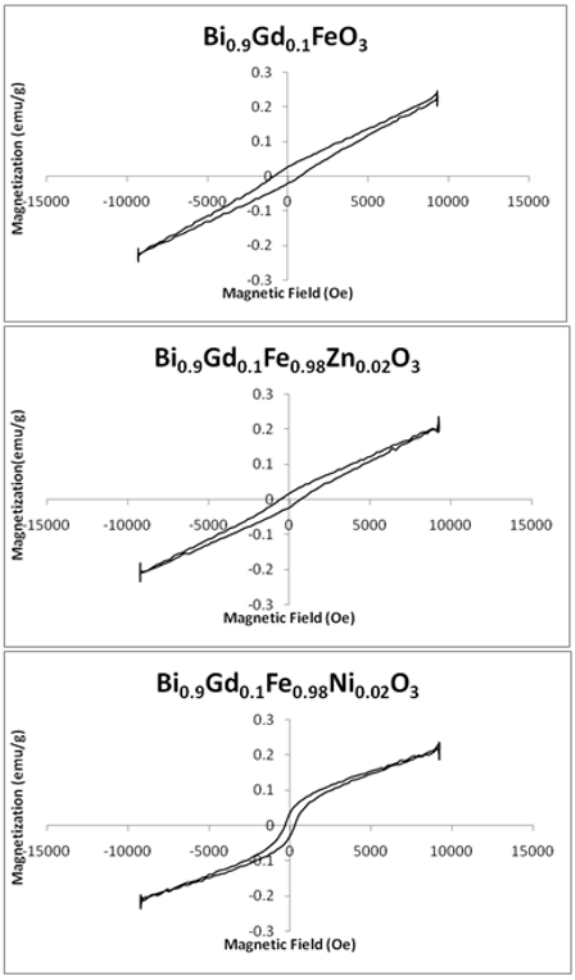

Fig. 4. The hysteresis loops of the Gd-doped compounds

4 Conclusion

We have prepared bismuth ferrite doped samples via the solid-state reaction method. Ca^{2+} or Gd^{3+}, were used to substitute for Bi^{3+} at the A-site of bismuth ferrite aiming to stabilize the perovskite phase that helps to decrease bismuth volatilization, while Zn^{2+} and Ni^{2+} were selected to substitute for Fe^{3+} at the B-site. XRD patterns confirmed the formation of the rhombohedral perovskite $BiFeO_3$ phase accompanied by some impurity phases such as $Bi_2Fe_4O_9$ and $Bi_{25}FeO_{40}$. Doping A-site with Ca^{2+} ions was found to stabilize the perovskite structure by suppressing impurity phases, while doping B-site with Nickel was found to enlarge the degree of distortion. The presence of impurity phases in the Gd^{3+} doped samples is due to the large atomic weights of gadolinium and samarium.

The diamagnetic A-site doping with the biggest ionic radius ions such as Gd^{3+} (r=1.053Å) has been found to be the most effective in the suppression of the spiral spin structure of bismuth ferrite and hence the appearance of weak ferromagnetism. Further, the charge compensation due to substitution of Bi^{3+} by Ca^{2+} (ions with different oxidation number) can be achieved by the formation of oxygen vacancies, which could increase the canting of the antiferromagnetically ordered spins and give rise to an increase in magnetization. We found that lattice distortion is the major cause behind

the significant increase in the net magnetization at room temperature. The wide loops observed for Gd-doped samples are due to the presence of defects in the crystal structure and the presence of higher concentration of second phases than those observed for other substitutions. This will help more in trapping (pinning) the magnetic flux lines leading to this loop opening.

Doping A-site was found to increase the coercivity and the remnant magnetization of bismuth ferrite, while doping B-site was found to decrease the coercivity field values and to increase the remnant magnetization values of the A-site doped samples in our work.

References

1. Y.H. Chu, R. Ramesh et al Nat. Mater **7**, 478 (2008)
2. C. Ederer and N. Spaldin, Phys. Rev. * **71**, 224103 (2005)
3. G.L.Yuan, S.W. Or, Y.P. Wang, Z.G. Liu, J.M. Liu, Sol. State Comm. **138** 76-81 (2006)
4. S. Basu, M. Pal and D. Chakravorty, J. Magn. Magn. Mat. **320** 3361-3365 (2008).
5. S.-H. Kim, J.-W. Jeong, J.-W. Lee and S.C. Shin, Thin Solid Films **517**, 2749-2752 (2009).
6. V. L. Mathe, J. Magn. Magn. Mater. **263**, 344 (2003)
7. V. L. Mathe, K. Patankar, R. Patil and C. Lokhande, J. Magn. Magn. Mater. 270,380 (2004).
8. J. Kim, S. Kim and W. Kim, Mater. Letters **59**, 4006 (2005).
9. Y. Wang, G. Yuan, X. Chen, J-M Liu and Z. Liu', J. Phys. D: Appl. Phys. **39** 2019 (2006)
10. Manoj Kumar and K. L.Yadav, J. Phys.: Condens. Matter **18** L503 (2006)
11. Mansour Al-Haj, Cryst. Res. Technol. 45 89 (2010).
12. R. Rai, I. Bdikin, M. Valente and A. KholkinMater. Chem. and Phys. **119** 539 (2010).
13. F. Qian, J. Jiang, D. Jiang, W. Zhang and J. Liu, J. Phys. D: Appl. Phys. **43** 25403 (2010).
14. V. Khomchenko, J. Paixao, V. Shvartsman, P. Borisov, W. Kleemann, D. Karpinsky and A.L. Kholkin, Scripta Materialia **62**, 238-241 (2010)
15. F. Azougha, R. Freer, M. Thrall, R. Cernik, F. Tuna and D. Collison, J. of the European Ceramic Society **30** 727 (2010)
16. V. A. Khomchenko, V.V. Scvartsman, P. Borisov, W. Kleemann, D.A. Kiselev, I.K. Bdikin, J.M.Vieira and A. L. Kholkin, J. Phys D: Appl. Phys, **42** (2009) 045418 (6pp).
17. M. Kumar and K. Yadav, J. Phys.: Condensed Matt. 18 L503 (2006).
18. R. D. Shanon, Acta Cryst A**32** 751 (1976)
19. R. Mishra, Dillip K. Pradham, R. N.P. Choudhary and A. Banerjee, J. Magn. Magn. Mat. **320**, 2602-2607 (2008)
20. D. Mauurya, H. Thota, A. Garg, B. Pandey, P. Chand and H. C. Verma, J. Phys.: Cond. Matt. **21** 26007 (2009)